Doping-induced variation of anomalous Hall effect in the magnetic Weyl-Kondo metal candidate $CeCo_{1-x}Fe_xGe_3$

Tomomi Furuhashi,[1,*] Keisuke Hozawa,[1] Yusuke Kozuka,[2]
Yoshihiro Tsujimoto,[2] Kazunari Yamaura,[2] and Jun Fujioka[3,4]

[1] *Graduate School of Science and Technology, University of Tsukuba, Tsukuba, Ibaraki 305-8573, Japan*

[2] *Research Center for Materials Nanoarchitechtonics (MANA), National Institute for Materials Science (NIMS), Namiki, Tsukuba, Ibaraki 305-0044, Japan*

[3] *Department of Materials Science, University of Tsukuba, Tsukuba, Ibaraki 305-8573, Japan*

[4] *Research Center for Organic-Inorganic Quantum Spin Science and Tchnology (OIQSST), University of Tsukuba, Tsukuba, Ibaraki 305-8573, Japan*

(Dated: October 22, 2025)

Abstract

We have investigated the doping-induced variation of magnetic and charge transport properties of single crystalline $CeCo_{1-x}Fe_xGe_3$ with a noncentrosymmetric tetragonal $BaNiSn_3$-type structure. The magnetization measurements revealed that, with increasing doping level x, the antiferromagnetic phase for $x = 0$ turns into a ferromagnetic one at $x = 0.15$, a cluster-glass like phase at $x = 0.46$, and eventually evolves into a paramagnetic phase above $x = 0.67$. For $0 \leq x < 0.46$ wherein the electrical resistivity shows the Fermi liquid behavior, the coefficient of the T^2-term of resistivity is small for $0 \leq x \leq 0.33$ but increases sharply at around $x \sim 0.42$, indicating the enhancement of density of state near the Fermi energy. Hall resistivity measurements indicate that, at 2 K in the ferromagnetic phase, the anomalous Hall conductivity remains nearly constant over the range $0.15 \leq x \leq 0.42$ but markedly decreases with increasing x beyond 0.42. Notably, an anomalous Hall component that is not proportional to magnetization is observed for $x \geq 0.42$. It is anticipated that the Berry curvature in momentum space significantly changes across the transition from the ferromagnetic phase to cluster-glass like phase, driven by a change in the Kondo hybridization in the present materials.

INTRODUCTION

The quantum phenomena arising from the interplay between topology and electron correlation in solids have attracted great interest in condensed matter physics. One of the most prominent examples is the correlated Weyl semimetal, where relativistic electrons exhibit a variety of collective phenomena associated with the Mott transition or heavy-fermion behavior. A characteristic feature of Weyl semimetals is the emergence of the Weyl nodes near the Fermi energy, which correspond to the source or the sink of the Berry curvature in momentum space [1–4]. In particular, the Berry curvature acts as the fictitious magnetic field to the conduction electrons [5], leading to significant intrinsic anomalous Hall effects, anomalous Nernst effects [6], and nonlinear Hall effects [7, 8]. On the other hand, a feature of strongly correlated electrons is the emergence of various electronic orderings such as magnetic, orbital and charge ordering, whose phase transitions are often accompanied by the dramatic reconstruction of electronic structure. Accordingly, strongly correlated Weyl semimetals provide a fertile playground for exploring emergent quantum states and transi-

tions. A prototypical example is d-electron-correlated electron systems in proximity to the Mott transition [2, 9–14]. For example, it is argued that antiferromagnetic Weyl semimetallic phase appears in a narrow phase space between the antiferromagnetic Mott insulating phase and the paramagnetic metallic phase in the pyrochlore iridates. In particular, several Weyl semimetallic phases compete with each other near the Mott criticality, and their transitions can be induced by the application of magnetic field or hydrostatic pressure, which manifest as significant variation of the anomalous Hall response [12, 15].

Recent theoretical studies predict that the heavy-mass quasiparticles in heavy-fermion systems can also induce a Weyl semimetallic phase, that is, Weyl-Kondo semimetal. For example, it has been argued that Weyl-Kondo semimetallic states are responsible for a giant spontaneous Hall effect in the noncentrosymmetric $Ce_3Bi_4Pd_3$ [16–18]. Moreover, a large anomalous Hall/Nernst effect in the ferromagnetic USbTe [19] and $UCo_{0.8}Ru_{0.2}Al$ [20] has been also understood from the Weyl semimetallic state originating from U-5f electrons. In heavy-fermion systems, the electronic state often undergoes significant changes due to the variation of Kondo hybridization [21–24]. Consequently, the Berry curvature in magnetic Weyl-Kondo metals would also significantly change, a subject that has not been sufficiently explored so far. In particular, it is still unclear whether topological phase transitions due to magnetic fields, similar to those observed in the Weyl semimetal near the Mott transition, also occur near the suppression of magnetic order in heavy-fermion systems.

In this context, the heavy-fermion compound $CeCo_{1-x}Fe_xGe_3$ is a promising candidate for exploring the interplay between magnetism and Dirac/Weyl electrons as the Kondo hybridization is tuned. $CeCo_{1-x}Fe_xGe_3$ crystallizes in the noncentrosymmetric tetragonal $BaNiSn_3$-type structure with space group $I4mm$, as shown in Fig. 1(a) [25–28]. The corners and the body center of the tetragonal structure are occupied by Ce-atoms, which show 4f-magnetic-moment with the easy axis anisotropy along the c-axis for $x = 0$ [29–31]. At zero magnetic field, $CeCoGe_3$ exhibits three successive antiferromagnetic transitions at T_{N1}=21 K, T_{N2}=12 K, and T_{N3}=8 K, respectively [25, 26, 30]. Neutron scattering studies on single crystals have identified the propagation vectors as q=(0, 0, 2/3) for $T_{N2} < T < T_{N1}$, q=(0, 0, 5/8) for $T_{N3} < T < T_{N2}$, and q=(0, 0, 1/2) for $T < T_{N3}$ [30]. Figure 1(a) illustrates an example of the magnetic structure with the propagation vector q=(0, 0, 2/3). The nonmagnetic Co-3d states are hybridized with the Ce-4f states [26, 32, 33], and the partial substitution of Co with Fe enhances the Kondo hybridization [34]; in $CeCo_{1-x}Fe_xGe_3$, the

magnetic ordering is suppressed with increasing x and vanishes around $x \sim 0.6$ [28, 34–37]. Recent theoretical studies argue that several Weyl nodes can emerge near the Fermi level due to the noncentrosymmetric crystal structure [38, 39]. Given these properties, $CeCo_{1-x}Fe_xGe_3$ appears to be an excellent platform to explore how the transport property of Dirac/Weyl electrons evolves as the Kondo hybridization strength is changed. However, there is no report on the magneto-transport property for the $CeCo_{1-x}Fe_xGe_3$ $(0 < x < 1)$ to the best of our knowledge, so far [19]. To precisely characterize the magnetic/magneto-transport property in materials with relatively large magnetic anisotropy, measurements on single crystalline samples are essential. Here, we investigated the doping-induced variation of magnetization, resistivity and Hall resistivity to get an insight into the variation of Berry curvature characteristic of Weyl-Kondo semimetal in $CeCo_{1-x}Fe_xGe_3$ single crystals.

METHODS

Single crystals of $CeCo_{1-x}Fe_xGe_3$ with $x < 0.5$ were grown by the Bi-flux method [26, 40]. The starting materials were mixed with the molar ratio Ce : Co : Fe : Ge : Bi = $1 : 1 - x : x : 3 : 10$–15, placed in alumina crucibles. The crucible sealed under vacuum in a quartz tube, was kept at 1050 °C for 24 h and was subsequently cooled down to 650–850 °C over 130 h. Then, the sealed ampoule was centrifuged to remove the Bi-flux. To obtain samples of sufficient size for magnetization measurements, single crystals of $CeCo_{1-x}Fe_xGe_3$ with $x > 0.6$ were grown by Sn-flux methods. The synthesis procedure was similar to that for Bi-flux, with an initial composition of Ce : Co : Fe : Ge : Sn = $1.2 : 1 - x : x : 3.5$–$3.7 : 30$, a maximum temperature of 1130 °C, a cooling time of 130–310 h, and a quench temperature of 600 °C. The crystals were characterized by X-ray powder diffraction using a Rigaku X-ray diffractometer with Cu-K_α radiation [see Fig. S1] [41]. The doping level of Fe (x) is determined by the energy dispersive X-ray spectroscopy (EDX) analysis [see Fig. S2] [41]. The doping level exhibits relatively large sample-to-sample variation, whereas no significant spatial inhomogeneity was detected within a single sample [see Fig. S3].

Measurements of resistivity and Hall resistivity were performed using the standard four-terminal method. The measurements were done using the Physical Property Measurement System (Quantum Design) from 2 K to 300 K under the magnetic field up to 9 T. The magnetization measurements were performed using the Dynacool System equipped with the VSM

option from 2 K to 300 K under the magnetic field up to 9 T. Several samples with different shapes show nearly identical magnetization profiles, suggesting that the demagnetization factor is not significant.

RESULTS

Figure 1(b) shows the temperature dependence of magnetization for $CeCo_{1-x}Fe_xGe_3$ with various x for magnetic field (B) along the c-axis [see also Figs. S4 and S5] [41]. Magnetic transitions manifest as multiple anomalies in the magnetization for $x \leq 0.48$. For $x = 0$, the magnetization exhibits three anomalies at the transition into $q_z = 2/3$-phase, $q_z = 5/8$-phase, and $q_z = 1/2$-phase at T_{N1}=20 K, T_{N2}=11.6 K, and T_{N3}=6 K, respectively, which are roughly consistent with the previous reports [25, 26, 30]. For $x = 0.13$, the magnetization exhibits only two anomalies at T_{N1} and T_{N2}, whereas a single ferromagnetic transition is observed for $x = 0.19$ and 0.42. For $x = 0.48$, the temperature dependence of magnetization shows a broad hump-like structure around 6.7 K, whereas no clear anomaly is observed for $x = 0.76$. The magnetization curves for various x are shown in Fig. 1(c). For $x = 0$, the magnetization plateau due to $q_z = 5/8$ phase, $q_z = 2/3$ phase, and ferromagnetic phase are observed at 2 K as previously reported [26], while a simple ferromagnetic hysteresis with the saturation magnetization about 0.4 μ_B/f.u. is observed for $x = 0.19$. For $x = 0.48$, the magnetization curve no longer shows the ferromagnetic hysteresis and smoothly increases as a function of magnetic field. For $x = 0.76$, the magnetization exhibits nearly B-linear behavior characteristic of the paramagnetic state.

Figure 2(a) shows the magnetic phase diagram based on the results of magnetization. With increasing x, the transition temperature of the $q_z = 2/3$-phase decreases while those of $q_z = 5/8$- and $1/2$-phases rather increase with increasing x. At around $x = 0.15$, these phases evolve into the ferromagnetic phase, which is then likely replaced by a different state around $x = 0.46$. Overall, this suggests that the Kondo hybridization suppresses the RKKY interaction and magnetically ordered phase, in qualitatively agreement with the previous results [33, 34]. It is known that, in Ce-based ferromagnets, the increase of Kondo interaction tends to promotes the antiferromagnetic interaction before reaching the quantum critical point, which often causes the Kondo-cluster glass state [42, 43]. Therefore considering the broad hump-like anomaly in temperature dependence of magnetization as

well as the smooth MH-curve, it is likely that the Kondo-cluster glass state appears below 6 K in the present material. Although the results around $x = 0.5$–0.6 are missing due to the lack of single crystalline samples, $x = 0.67$ exhibits paramagnetic behavior in the range of 2–300 K (shown as a green cross in Fig. 2(a)). Therefore, the cluster-glass like phase likely vanishes around $x = 0.5$–0.6, which is consistent with previous reports [28, 34–37].

Figures 3(a) and (b) show the temperature dependence of resistivity (ρ_{xx}) at $B = 0$ T. All the samples show metallic behavior, and a clear kink is observed at the magnetic transition temperature for $x \leq 0.42$ [see Fig. 3(a)]. In contrast, no clear kinks are visible for $x \geq 0.46$ [see Fig. 3(b)]. For $x \leq 0.42$, ρ_{xx} shows the Fermi liquid behavior $\rho_{xx}(T) = AT^2 + \rho_0$ with A and ρ_0 being the constant and residual resistivity, respectively at low temperatures ($T < 5$ K) [see Fig. S6]. It is known that A is related to the density of states near the Fermi energy through the Kadowaki-Woods relation $A/\gamma^2 \sim 1.0 \times 10^{-5}\,\mu\Omega\mathrm{cm(K \cdot mol/mJ)}^2$ in various heavy-fermion systems [44]. Here, γ is the electronic specific heat coefficient. Fig. 2(b) shows the doping dependence of A. As a function of x, A gradually increases in the low doping regime but is sharply enhanced above $x \sim 0.4$, suggesting that the density of states near the Fermi energy increases significantly above $x \sim 0.4$ due to the delocalization of Ce-4f state. A similar behavior has been demonstrated in polycrystalline samples [34, 36]. For $x = 0.48$, $\rho_{xx}(T)$ exhibits a nearly T-linear behavior rather than the conventional Fermi liquid behavior at low temperatures [see the inset to Fig. 3(b)], which is often observed near the quantum critical point in heavy fermion systems [45, 46].

Figures. 4(a)–(d) show the magnetic field dependence of the Hall resistivity for $x = 0$, 0.19, 0.33, and 0.48, respectively. For $x = 0$, ρ_{yx} is small and exhibits an almost linear dependence on magnetic field (B) at 100 K, but is remarkably enhanced at 20 K, showing the nonlinear B-dependence [see Fig. 4(a)]. With further lowering temperature, ρ_{yx} is rather reduced, and a jump (or kink) due to the metamagnetic transition becomes remarkable. For $x = 0.19$ which lies in ferromagnetic phase, ρ_{yx} shows a step around $B = 0$, followed by a nearly linearly increase at a higher field region, corresponding to the anomalous Hall effect and ordinary Hall effect, respectively. The sign of the anomalous Hall resistivity is positive at 15 K but changes to negative at low temperatures [see the inset to Fig. 4(b)]. A similar behavior is observed for $x = 0.33$; the sign of anomalous Hall effect is reversed by changing the temperature, while the sign of ordinary Hall effect remains to be positive at all temperatures [see Fig. 4(c)]. For $x = 0.48$, ρ_{yx} exhibits a sign change, similar to the

anomalous Hall component for $x = 0.19$ and 0.33, while complex behavior emerges near and below T_N in the low field regime; a peak feature appears around 2 T and 6 K, which evolves into a dip structure below 4 K. Although ρ_{yx} for $x = 0$ and $x = 0.48$ exhibit complicated field-dependence, it is likely that, in the low-field regime below 1 T, the primary contribution to ρ_{yx} is commonly ascribed to the anomalous Hall term.

To qualitatively evaluate the temperature dependence of the anomalous Hall term, we plot ρ_{yx} at 0.2 T (ρ_{yx}(0.2 T)) as a function of temperature in Fig. 4(e). For $x = 0$, with decreasing temperature, ρ_{yx}(0.2 T) gradually increases, maximizes near or slightly higher than T_N and finally becomes vanishingly small below 10 K. For $x = 0.19$ and 0.33, ρ_{yx}(0.2 T) shows a maximum near T_C analogous to the behavior of $x = 0$, but its sign changes to negative below 15 K. A similar behavior is observed for $x = 0.48$. To visualize the doping evolution of ρ_{yx}(0.2 T), we show the contour plot of ρ_{yx}(0.2 T) on the x-T plane in Fig. 4(f). Above the transition temperature, ρ_{yx}(0.2 T) is positive in wide range of temperatures and doping levels. In particular, the positive region extends up to about 100 K for $x = 0$, which gradually shrinks with increasing x and nearly vanishes around $x = 0.48$. In the magnetically ordered phase, ρ_{yx}(0.2 T) is negligibly small in the antiferromagnetic phase for $0 \leq x < 0.15$, whereas it becomes significantly large in magnitude and negative in sign both in the ferromagnetic phase and cluster-glass like phase for $0.15 \leq x \leq 0.48$. In heavy fermion systems, it is well known that the anomalous Hall effect arises predominantly from incoherent skew scattering in the vicinity of, and above, the magnetic transition temperature or the coherence temperature. In contrast, at lower temperatures, the anomalous Hall effect is mainly attributed to coherent skew scattering or intrinsic mechanisms [47–49]. Indeed, it is demonstrated that the temperature dependence of ρ_{yx}(0.2 T) exhibits a broad peak near and above the transition temperature of antiferromagnetic ordering in $CeAl_3$ and $CeCu_2Si_2$ [49]. In this context, it is likely that the substantial positive component near and above the magnetic transition temperature originates from the incoherent skew scattering, whereas the negative component in the ferromagnetic/cluster-glass like phase can be attributed to coherent skew scattering or intrinsic mechanisms in the present system.

To clarify the mechanism of negative component, we plot the anomalous Hall conductivity σ_{xy}^M at 2 K, defined as the zero-field Hall conductivity ($B = 0$ T), as a function of longitudinal electrical conductivity σ_{xx} for several ferromagnetic samples with $0.15 \leq x \leq 0.33$ [see Figs. 5(a) and 6(a)]. σ_{xy}^M at 2 K is found to be almost independent of σ_{xx}, indicating that the

negative component of σ_{xy}^{M} originates from the intrinsic mechanism, i.e. the Berry curvature in the momentum space [50, 51].

To separate the contribution from the ordinary Hall effect and anomalous Hall effect, we analyzed the Hall conductivity in both the ferromagnetic phase and the cluster-glass like phase using the following formula

$$\sigma_{xy} = \sigma_{xy}^{N} + \sigma_{xy}^{M} + \sigma_{xy}^{res} \tag{1}$$

The first, second, and third terms represent the ordinary Hall term ($\sigma_{xy}^{N} = \sum_i \frac{n_i e \mu_i^2 B}{1+(\mu_i B)^2}$), the anomalous Hall term in proportion to M ($\sigma_{xy}^{M} = S_A M$), and the residual component (σ_{xy}^{res}), which is neither proportional to B nor to M, respectively. Here, n_i and μ_i are the density and mobility of i-th carrier, respectively, and S_A is the anomalous Hall coefficient. The analyzed results at 2 K for $x = 0.15$, $x = 0.29$, $x = 0.33$, $x = 0.42$ and $x = 0.48$ are shown in Figs. 5 (a)–(c). For $x = 0.15$, $x = 0.29$ and $x = 0.33$, which is located in the middle of ferromagnetic phase, σ_{xy} is well reproduced by the simple summation of σ_{xy}^{N} and σ_{xy}^{M} ($\sigma_{xy}^{N} + \sigma_{xy}^{M}$) [see Fig. 5(a)]. On the contrary, for $x = 0.42$, which is the ferromagnetic phase in vicinity to the cluster-glass like phase, a small deviation between σ_{xy} and $\sigma_{xy}^{N} + \sigma_{xy}^{M}$ is seen below 2 T ($|B| < 2$ T) [see Fig. 5(b)]. The deviation becomes more significant for $x = 0.48$ which lies in the cluster-glass like phase [see Fig. 5(c)]; σ_{xy} is well reproduced by $\sigma_{xy}^{N} + \sigma_{xy}^{M}$ above 3 T, whereas a significant deviation is observed near 2 T, indicating a substantial contribution from σ_{xy}^{res}. Figures 5(d)–(f) show the magnetic field dependence of σ_{xy}^{res} at 2 K for representative compositions. Although there is no systematic or reproducible peak/dip for $0.15 \leq x \leq 0.33$, pronounced peaks are observed at $x = 0.42$ and $x = 0.48$.

DISCUSSION

Figures 6(b) and (c) summarize the doping dependence of σ_{xy}^{M} and σ_{xy}^{res} as well as the magnetization at 2 K. The magnetization measured at 7 T is nearly constant for $0.15 \leq x \leq 0.33$ and slightly decreases for $x \sim 0.42$. In contrast, σ_{xy}^{M} remains nearly constant for $0.15 \leq x \leq 0.33$ but drops abruptly at $x \sim 0.42$, indicating that the Berry curvature in momentum space rapidly changes around $x = 0.42$. As previously mentioned, the A-coefficient sharply increases around $x = 0.42$, which is attributed to the delocalization of Ce-4f electrons [see Fig. 2(b)]. The theoretical study argues that the structure of Weyl

nodes is reconstructed when the Ce-4f state is hybridized with the states near the Fermi energy in $CeCo_{1-x}Fe_xGe_3$ [38]. Therefore, it is likely that the Berry curvature in momentum space changes rapidly with respect to x around $x = 0.42$, resulting in the suppression of σ_{xy}^{M}.

Figure 6(c) shows the maximum of $-\sigma_{xy}^{res}(-\sigma_{xy}^{res,max})$ plotted as a function of x. $-\sigma_{xy}^{res}$ is nearly constant for $0.15 \leq x \leq 0.33$ and rises above $x = 0.42$, implying that σ_{xy}^{res} is also closely linked to the reconstruction of the Ce-4f electronic state. A similar peak/dip structure of Hall conductivity is often seen in magnetic Weyl semimetals [52, 53]. For example, in the perovskite-type $EuTiO_3$, an anomalous Hall component not proportional to magnetization has been observed during the field-induced spin-reorientation process, which is attributed to the field-induced shift of Weyl nodes located in proximity to the Fermi energy [52]. In the present system, at $x = 0.48$, the cluster-glass like state seems to change into the forced ferromagnetic phase by the application of a magnetic field. It is anticipated that the structure of Weyl nodes is modulated in the course of the magnetization process, leading to the non-monotonic field dependence of anomalous Hall effect. Another possibility is the field-induced variation of Kondo hybridization. It is known that Ce-based heavy-fermion systems on the verge of the quantum critical point often show the field-induced variation of Kondo hybridization. A prominent example is $CeRu_2Si_2$, a paramagnetic compound close to a quantum critical point, which exhibits a metamagnetic-like transition into the enforced ferromagnetic phase [54, 55]. This phenomenon is attributed to the field-induced suppression of Kondo hybridization. In the present case, a slight change in the Kondo hybridization due to the magnetic field could change the Berry curvature in the momentum space. Such doping/field-sensitive anomalous Hall effect may be a hallmark of Weyl semimetal close to quantum phase transition in a heavy-fermion system.

In summary, we have investigated the magnetic and charge transport properties for heavy-fermion systems $CeCo_{1-x}Fe_xGe_3$. Magnetization measurements reveal that the magnetic ordering evolves from an antiferromagnetic phase to a ferromagnetic phase around $x = 0.15$, and then to a cluster-glass like phase around $x = 0.46$. In particular, the transition temperature of magnetic ordering gradually decreases with increasing x, and finally the paramagnetic state appears around $x = 0.5$–0.6. This is in parallel with enhanced T^2 coefficient of resistivity, implying that the delocalized Ce-4f state starts to be formed near the Fermi energy for $x > 0.42$. Above the magnetic transition temperature, the Hall resistivity in the low field regime is likely dominated by the anomalous Hall effect of incoherent skew scattering mecha-

nism, while the intrinsic anomalous Hall effect is observed in the ferromagnetic/cluster-glass like phase. The magnitude of anomalous Hall conductivity is nearly x-independent for $0.1 \leq x \leq 0.33$, but rapidly decreases for $x \geq 0.42$. Moreover, the peculiar anomalous Hall response emerges in and near the cluster-glass like phase, which cannot be explained by conventional contributions that scale monotonically with magnetic field or magnetization. These results suggest that the Weyl nodes near the Fermi energy undergo significant changes under the influence of external fields or varying doping levels, especially in the vicinity of the localization-delocalization crossover of the Ce-4f state.

ACKNOWLEDGEMENTS

The EDX analysis was carried out with TM4000 (Hitachi High-Tech.) at R&D Center for Innovative Material Characterization and the Organization for Open Facility Initiatives, University of Tsukuba. This work was partly supported by Grant-In-Aid for Science Research (Nos. 18H01171, 21K18813, 22H01177, 25K01657) from the Mext, by Iketani Foundation for Materials Science and Engineering, Japan, by JST FOREST Program (Grant Number: JPMJFR203D) MANA is supported by World Premier International Research Center Initiative (WPI), MEXT, Japan and by JST SPRING (Grant Number: JPMJSP2124).

* furuhashi.tomomi.tkb_go@u.tsukuba.ac.jp

[1] S. Murakami, New J. Phys. **9**, 356 (2007).

[2] X. Wan, A. M. Turner, A. Vishwanath, and S. Y. Savrasov, Phys. Rev. B **83**, 205101 (2011).

[3] N. P. Armitage, E. J. Mele, and A. Vishwanath, Rev. Mod. Phys. **90**, 015001 (2018).

[4] Z. Fang, N. Nagaosa, K. S. Takahashi, A. Asamitsu, R. Mathieu, T. Ogasawara, H. Yamada, M. Kawasaki, Y. Tokura, and K. Terakura, Science **302**, 92 (2003).

[5] D. Xiao, M.-C. Chang, and Q. Niu, Rev. Mod. Phys. **82**, 1959 (2010).

[6] N. Nagaosa, J. Sinova, S. Onoda, A. H. MacDonald, and N. P. Ong, Rev. Mod. Phys. **82**, 1539 (2010).

[7] K. Kang, T. Li, E. Sohn, J. Shan, and K. F. Mak, Nat. Mater. **18**, 324 (2019).

[8] Q. Ma, S.-Y. Xu, H. Shen, D. MacNeill, V. Fatemi, T.-R. Chang, A. M. Mier Valdivia, S. Wu,

Z. Du, C.-H. Hsu, *et al.*, Nature **565**, 337 (2019).

[9] J.-M. Carter, V. V. Shankar, M. A. Zeb, and H.-Y. Kee, Phys. Rev. B **85**, 115105 (2012).

[10] W. Witczak-Krempa and Y. B. Kim, Phys. Rev. B **85**, 045124 (2012).

[11] K.-Y. Yang, Y.-M. Lu, and Y. Ran, Phys. Rev. B **84**, 075129 (2011).

[12] K. Ueda, T. Oh, B.-J. Yang, R. Kaneko, J. Fujioka, N. Nagaosa, and Y. Tokura, Nat. Commun. **8**, 15515 (2017).

[13] J. Fujioka, R. Yamada, M. Kawamura, S. Sakai, M. Hirayama, R. Arita, T. Okawa, D. Hashizume, M. Hoshino, and Y. Tokura, Nat. Commun. **10**, 362 (2019).

[14] R. Yamada, J. Fujioka, M. Kawamura, S. Sakai, M. Hirayama, R. Arita, T. Okawa, D. Hashizume, T. Sato, F. Kagawa, R. Kurihara, M. Tokunaga, and Y. Tokura, npj Quantum Mater. **7**, 13 (2022).

[15] K. Ueda, R. Kaneko, H. Ishizuka, J. Fujioka, N. Nagaosa, and Y. Tokura, Nat. Commun. **9**, 3032 (2018).

[16] S. Dzsaber, X. Yan, M. Taupin, G. Eguchi, A. Prokofiev, T. Shiroka, P. Blaha, O. Rubel, S. E. Grefe, H.-H. Lai, Q. Si, and S. Paschen, Proc. Natl. Acad. Sci. U.S.A. **118**, e2013386118 (2021).

[17] S. Dzsaber, D. A. Zocco, A. McCollam, F. Weickert, R. McDonald, M. Taupin, G. Eguchi, X. Yan, A. Prokofiev, L. M. K. Tang, B. Vlaar, L. E. Winter, M. Jaime, Q. Si, and S. Paschen, Nat. Commun. **13**, 5729 (2022).

[18] M. Braß, J. M. Tomczak, and K. Held, Phys. Rev. Research **6**, 033227 (2024).

[19] H. Siddiquee, C. Broyles, E. Kotta, S. Liu, S. Peng, T. Kong, B. Kang, Q. Zhu, Y. Lee, L. Ke, H. Weng, J. D. Denlinger, L. A. Wray, and S. Ran, Nat. Commun. **14**, 527 (2023).

[20] T. Asaba, V. Ivanov, S. M. Thomas, S. Y. Savrasov, J. D. Thompson, E. D. Bauer, and F. Ronning, Sci. Adv. **7**, eabf1467 (2021).

[21] G. R. Stewart, Rev. Mod. Phys **56**, 755 (1984).

[22] Q. Si and F. Steglich, SCIENCE **329**, 1161 (2010).

[23] Q. Si and S. Paschen, Phys. Status Solidi B **250**, 425 (2013).

[24] S. Doniach, Physica B+C **91**, 231 (1977).

[25] V. K. Pecharsky, O.-B. Hyun, and K. A. Gschneidner, Phys. Rev. B **47**, 11839 (1993).

[26] A. Thamizhavel, T. Takeuchi, T. D. Matsuda, Y. Haga, K. Sugiyama, R. Settai, and Y. Ōnuki, J. Phys. Soc. Jpn. **74**, 1858 (2005).

[27] H. Yamamoto, H. Sawa, and M. Ishikawa, Phys. Lett. A **196**, 83 (1994).

[28] S. de Medeiros, S. Bud ' ko, M. Fontes, M. Continentino, and E. Baggio-Saitovitch, J. Magn. Magn. Mater **226–230**, 152 (2001).

[29] K. Kaneko, N. Metoki, T. Takeuchi, T. D. Matsuda, Y. Haga, A. Thamizhavel, R. Settai, and Y. Ōnuki, J. Phys.: Conf. Ser. **150**, 042082 (2009).

[30] M. Smidman, D. T. Adroja, A. D. Hillier, L. C. Chapon, J. W. Taylor, V. K. Anand, R. P. Singh, M. R. Lees, E. A. Goremychkin, M. M. Koza, V. V. Krishnamurthy, D. M. Paul, and G. Balakrishnan, Phys. Rev. B **88**, 134416 (2013).

[31] T. Inagaki, M. Matsumura, M. Mizoo, Y. Kawamura, H. Kato, and T. Nishioka, J. Phys.: Conf. Ser. **400**, 032026 (2012).

[32] A. Thamizhavel, H. Shishido, Y. Okuda, H. Harima, T. D. Matsuda, Y. Haga, R. Settai, and Y. Ōnuki, J. Phys. Soc. Jpn. **75**, 044711 (2006).

[33] P. Li, H. Ye, Y. Hu, Y. Fang, Z. Xiao, Z. Wu, Z. Shan, R. P. Singh, G. Balakrishnan, D. Shen, Y.-F. Yang, C. Cao, N. C. Plumb, M. Smidman, M. Shi, J. Kroha, H. Yuan, F. Steglich, and Y. Liu, Phys. Rev. B **107**, L201104 (2023).

[34] P. Skokowski, K. Synoradzki, M. Werwiński, A. Bajorek, G. Chełkowska, and T. Toliński, J. Alloys Compd. **787**, 744 (2019).

[35] P. Skokowski, K. Synoradzki, and T. Toliński, Acta Phys. Pol. A **131**, 1000 (2017).

[36] P. Skokowski, K. Synoradzki, and T. Toliński, J. Alloys Compd. **810**, 151850 (2019).

[37] P. Skokowski, K. Synoradzki, M. Reiffers, A. Dzubinska, S. Rols, S. Arapan, D. Legut, and T. Toliński, Intermetallics **153**, 107776 (2023).

[38] V. Ivanov, X. Wan, and S. Y. Savrasov, Phys. Rev. B **103**, L041112 (2021).

[39] Y. Fang, L. Chen, A. Prokofiev, I. Robredo, J. Cano, M. G. Vergniory, S. Paschen, and Q. Si, Magnetic Weyl-Kondo semimetals induced by quantum fluctuations, *arXiv*, 2403.02295 (2024), arXiv:2403.02295 [cond-mat.str-el].

[40] M. Kakihana, H. Akamine, K. Tomori, K. Nishimura, A. Teruya, A. Nakamura, F. Honda, D. Aoki, M. Nakashima, Y. Amako, K. Matsubayashi, Y. Uwatoko, T. Takeuchi, T. Kida, M. Hagiwara, Y. Haga, E. Yamamoto, H. Harima, M. Hedo, T. Nakama, and Y. Ōnuki, J. Alloys Compd. **694**, 439 (2017).

[41] See Supplemental Material for details on sample characterization and magnetization measurements.

[42] T. Westerkamp, M. Deppe, R. Küchler, M. Brando, C. Geibel, P. Gegenwart, A. P. Pikul, and F. Steglich, Phys. Rev. Lett. **102**, 206404 (2009).

[43] T. Vojta, J. Low Temp. Phys. **161**, 299 (2010).

[44] K. Kadowaki and S. Woods, Solid State Commun. **58**, 507 (1986).

[45] G. R. Stewart, Rev. Mod. Phys. **73**, 797 (2001).

[46] M. Brian Maple, R. E. Baumbach, N. P. Butch, J. J. Hamlin, and M. Janoschek, J. Low Temp. Phys. **161**, 4 (2010).

[47] A. Fert, P. Pureur, A. Hamzic, J. P. Kappler, and P. M. Levy, Phys. Rev. B **32**, 7003 (1985).

[48] A. Fert and P. M. Levy, Phys. Rev. B **36**, 1907 (1987).

[49] Y. Ōnuki, T. Yamazaki, T. Omi, I. Ukon, A. Kobori, and T. Komatsubara, J. Phys. Soc. Jpn. **58**, 2126 (1989).

[50] S. Onoda, N. Sugimoto, and N. Nagaosa, Phys. Rev. B **77**, 165103 (2008).

[51] T. Miyasato, N. Abe, T. Fujii, A. Asamitsu, S. Onoda, Y. Onose, N. Nagaosa, and Y. Tokura, Phys. Rev. Lett. **99**, 086602 (2007).

[52] K. S. Takahashi, H. Ishizuka, T. Murata, Q. Y. Wang, Y. Tokura, N. Nagaosa, and M. Kawasaki, Sci. Adv. **4**, eaar7880 (2018).

[53] J. Chen, H. Li, B. Ding, P. Chen, T. Guo, X. Xu, D. Zheng, H. Zhang, X. Xi, and W. Wang, Adv. Funct. Mater. **32**, 2107526 (2022).

[54] J.-X. Boucherle, F. Givord, S. Raymond, J. Schweizer, E. Leliévre-Berna, P. Lejay, and G. Fillion, J. Phys.: Condens. Matter **13**, 10901 (2001).

[55] R. Daou, C. Bergemann, and R. Julian, Phys. Rev. Lett. **96**, 026401 (2006).

[56] K. Momma and F. Izumi, J. Appl. Crystallogr. **44**, 1272 (2011).

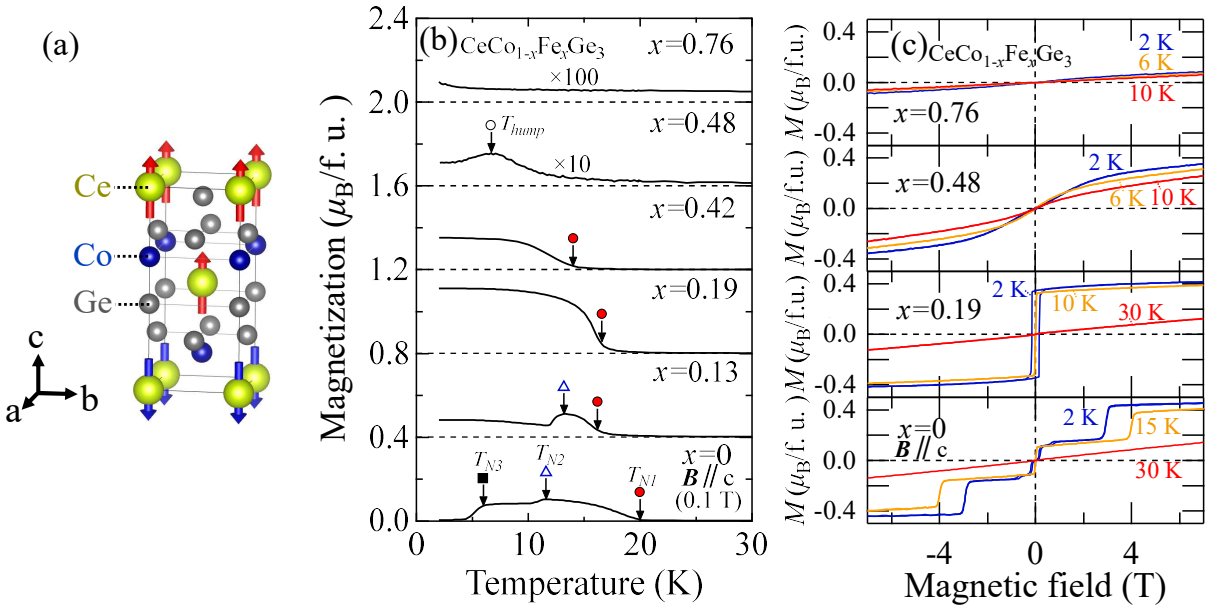

FIG. 1. (a) The illustration of the crystal structure of $CeCoGe_3$with up-up-down-type magnetic structure (q_z=(0, 0, 2/3)) [56]. Arrows denote the Ce-4f magnetic moment. (b) The temperature and (c) magnetic field dependence of magnetization for the magnetic field (B) along the c-axis for representative compositions of $CeCo_{1-x}Fe_xGe_3$. Solid circles, open triangles, and solid squares denote the magnetic transition temperature at T_{N1}, T_{N2}, and T_{N3}, respectively. Open circles denote the characteristic temperature of cluster-glass like state. The transition temperature was determined from the kink in the temperature dependence of magnetization. When it was difficult to determine the transition temperature by the kink, the transition temperature was determined using the peak of the second derivative of magnetization with respect to temperature.

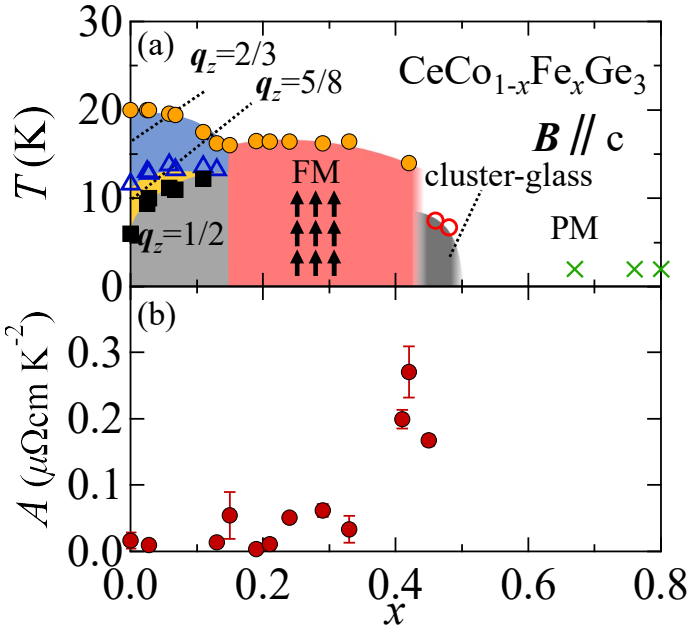

FIG. 2. (a) The magnetic phase diagram for $CeCo_{1-x}Fe_xGe_3$. Here, q_z represents the wave number of magnetic modulation along the c-axis. Solid circles, open triangles, and solid squares denote the magnetic transition temperature at T_{N1}, T_{N2}, and T_{N3}, respectively. Open circle denote the transition temperature of cluster-glass like state. Cross denotes the samples for which no magnetic transition was observed in the 2–300 K range. (b) The A-coefficient in the T^2 term of the electrical resistivity as a function of x.

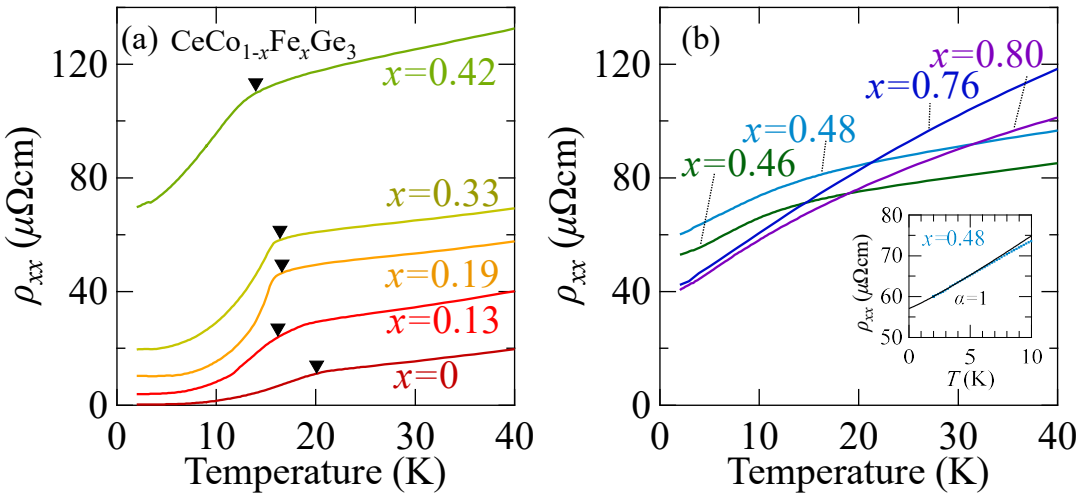

FIG. 3. The temperature dependence of resistivity (ρ_{xx}) at B=0 T for (a) $0 \leq x \leq 0.42$ and (b) $0.46 \leq x \leq 0.80$. Solid triangles denote the kink at the magnetic transition temperature determined from the temperature dependence of magnetization. The inset shows the magnified view of low-temperature region for $x = 0.48$. The solid line in the inset denotes the fitting-results by $\rho_{xx}(T) = AT^{\alpha} + \rho_0$ ($\alpha = 1$).

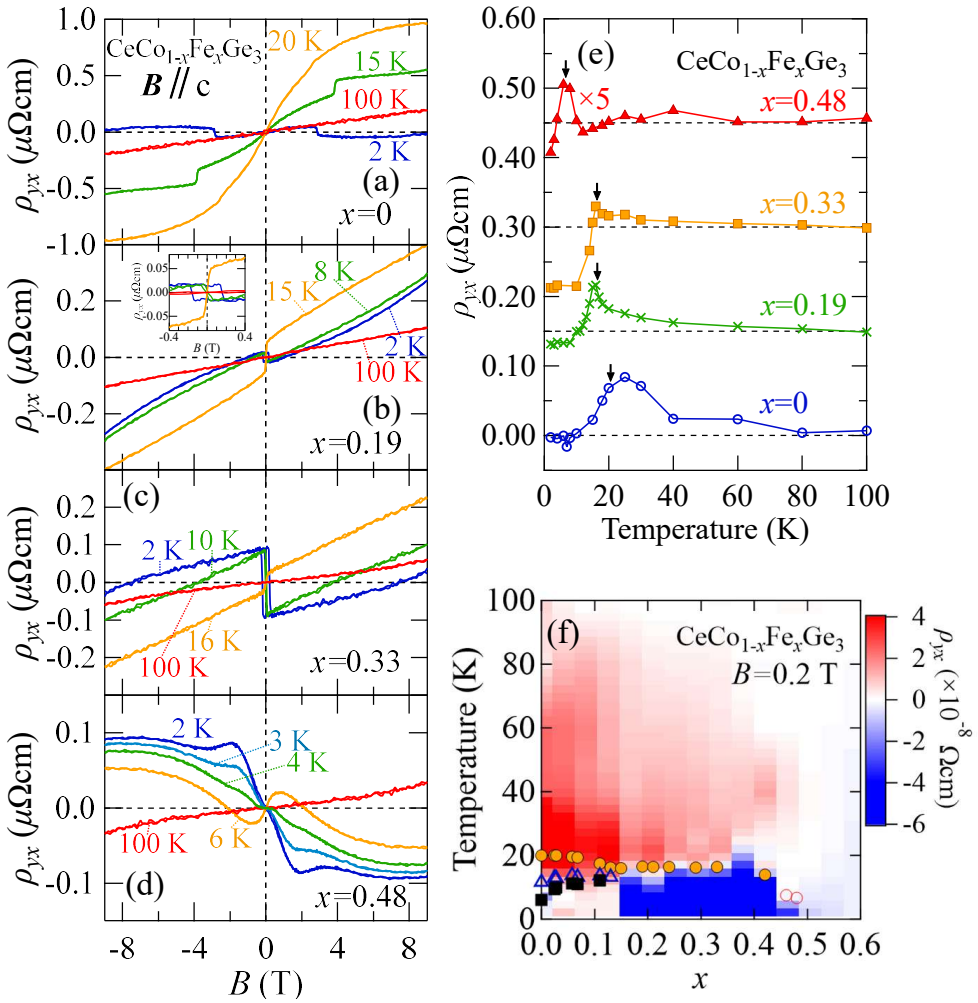

FIG. 4. The magnetic field dependence of the Hall resistivity for $CeCo_{1-x}Fe_xGe_3$ with (a) $x = 0$, (b) $x = 0.19$, (c) $x = 0.33$ and (d) $x = 0.48$. The inset to (b) is a magnified view of the low field region. (e) Temperature-dependence of ρ_{yx} at B=0.2 T for $x = 0$, 0.19, 0.33, and 0.48. Arrows denote the magnetic transition temperature. (f) The contour plot of ρ_{yx} at B=0.2 T in the x-T plane. Solid circles, open triangles, and solid squares denote the magnetic transition temperature at T_{N1}, T_{N2}, and T_{N3}, respectively. Open circles denote the transition temperature of cluster-glass like phase.

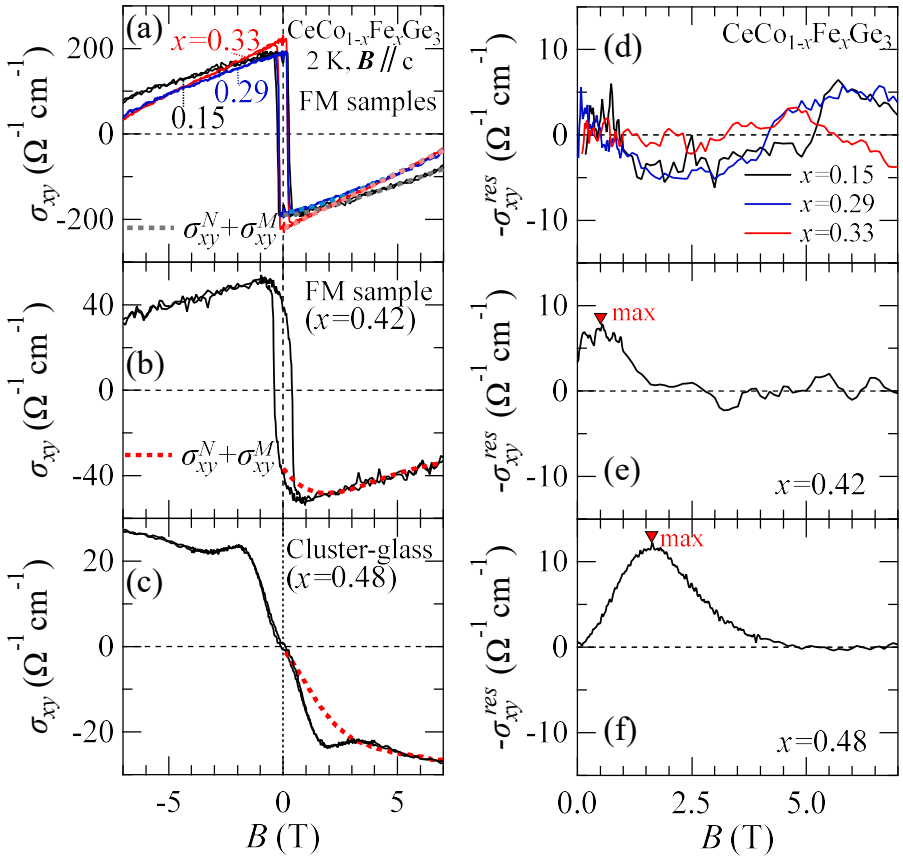

FIG. 5. The magnetic field dependence of Hall conductivity at 2 K for (a) the samples located in the middle of ferromagnetic phase ($x = 0.15$, $x = 0.29$, $x = 0.33$), (b) the sample located near the phase boundary ($x = 0.42$), and (c) the sample that in the cluster-glass like phase ($x = 0.48$) respectively. The dashed curve denotes the $\sigma_{xy}^{N} + \sigma_{xy}^{M}$. (d)–(f) The magnetic field dependence of Hall conductivity which is proportional neither to B nor to M ($-\sigma_{xy}^{res}$) corresponding to each composition shown in (a)–(c). The solid triangles denote the peak of $-\sigma_{xy}^{res}$.

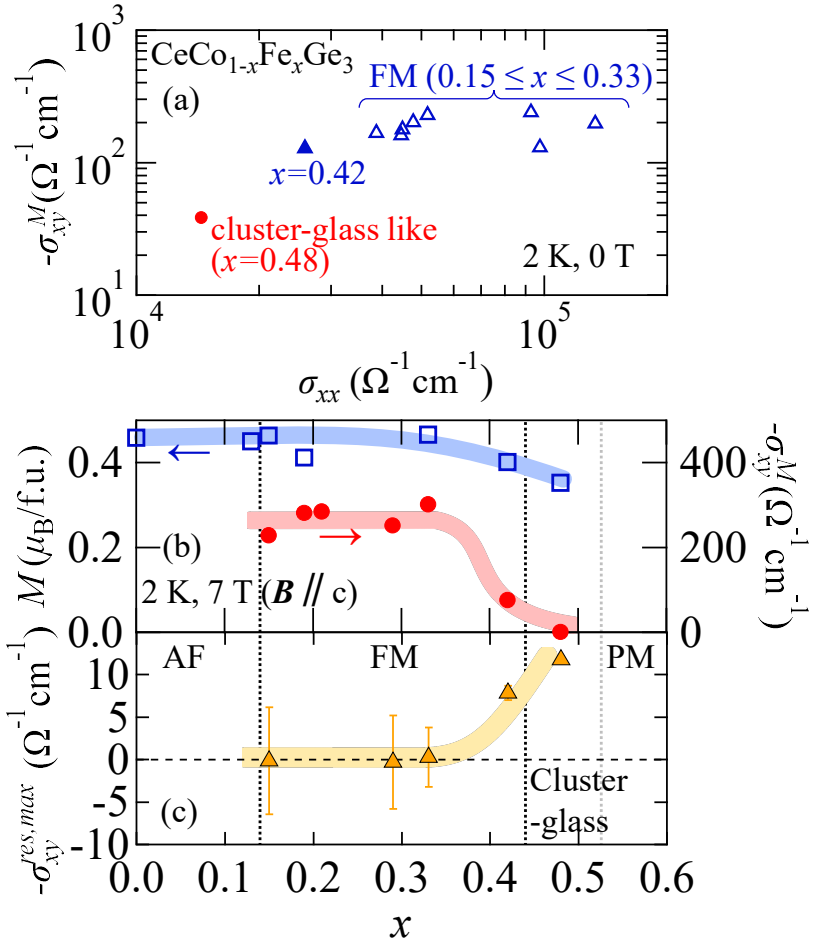

FIG. 6. (a) The anomalous Hall conductivity $-\sigma_{xy}^{M}$ at 2 K, which is defined by the Hall conductivity at B=0 T as a function of electrical conductivity σ_{xx}. Open triangles denote samples located in the middle of ferromagnetic phase ($0.15 \leq x \leq 0.33$), the solid triangle denote the sample located near the phase boundary ($x = 0.42$) and solid circle denote the sample that in the cluster-glass like phase ($x = 0.48$). (b) The magnetization at 2 K, 7 T (open squares) and Hall conductivity proportional to M (σ_{xy}^{M}) at 2 K, 7 T (solid circles), (d) The maximum value of the residual Hall conductivity at 2 K($-\sigma_{xy}^{res,max}$) as a function of x. Since systematically-changed peak/dip of $-\sigma_{xy}^{res}$ is not observed for $0.15 \leq x \leq 0.33$ [see also Fig. 5(d)], the maximum and minimum values of $-\sigma_{xy}^{res}$ are shown by error bars and their average values are plotted.